ACTUATORS

Actuation of untethered pneumatic artificial muscles and soft robots using magnetically induced liquid-to-gas phase transitions

Seyed M. Mirvakili[1]*, Douglas Sim[2], Ian W. Hunter[3], Robert Langer[1,4,5,6]

Copyright © 2020 The Authors, some rights reserved; exclusive licensee American Association for the Advancement of Science. No claim to original U.S. Government Works

Pneumatic artificial muscles have been widely used in industry because of their simple and relatively high-performance design. The emerging field of soft robotics has also been using pneumatic actuation mechanisms since its formation. However, these actuators/soft robots often require bulky peripheral components to operate. Here, we report a simple mechanism and design for actuating pneumatic artificial muscles and soft robotic grippers without the use of compressors, valves, or pressurized gas tanks. The actuation mechanism involves a magnetically induced liquid-to-gas phase transition of a liquid that assists the formation of pressure inside the artificial muscle. The volumetric expansion in the liquid-to-gas phase transition develops sufficient pressure inside the muscle for mechanical operations. We integrated this actuation mechanism into a McKibben-type artificial muscle and soft robotic arms. The untethered McKibben artificial muscle generated actuation strains of up to 20% (in 10 seconds) with associated work density of 40 kilojoules/meter^3, which favorably compares with the peak strain and peak energy density of skeletal muscle. The untethered soft robotic arms demonstrated lifting objects with an input energy supply from only two Li-ion batteries.

INTRODUCTION

Mimicking muscle-generated movements—such as locomotion, lifting, rotation, and bending—has been of great interest for application in robotics and electromechanical systems (*1*). To address this need, several categories of muscle-like actuators (known as artificial muscles) have been developed over the past several decades. Shape memory materials (excited via Joule heating, light, or induction heating) (*2*–*6*), dielectric elastomers (*7*, *8*), hydraulic actuators (*9*, *10*), highly oriented thermo-responsive polymers (*11*, *12*), conducting polymers (*13*, *14*), ionic polymer metal composites (*15*, *16*), and pneumatic actuators (*17*–*20*) are among the highly developed materials and devices for artificial muscles.

Owing to their simple design, pneumatic artificial muscles (PAMs) are among the most industrially applied and highly developed actuators. One of the early examples of soft pneumatic actuators is the McKibben artificial muscle, which is made of a compliant bladder confined within a braided jacket. Bending, torsional, and linear contractile dynamics have been demonstrated with PAMs (*21*). PAMs can generate up to 36% strain with energy and power densities of up to 200 kJ/m^3 and 1 MW/m^3, respectively (*22*).

Newer designs have improved the performance in aspects such as strain, manufacturability, and increased range of motions (*23*–*26*). However, one of the fundamental limitations of PAMs and soft robots for portable devices is the weight/size requirement of compressors, valves, and pumps. This issue is addressed to some extent by using alternative techniques to generate the required pressure for actuation. For example, combustion (e.g., butane/oxygen) (*24*), gas evolution reactions (e.g., hydrogen peroxide with platinum catalyst, consumption of oxygen and hydrogen with a fuel cell to make vacuum, or generating CO_2 from urea with a catalyzer) (*25*, *27*), chemically activating swelling/deswelling (e.g., pH-sensitive hydrogels) (*28*), and phase change materials (e.g., ethanol and paraffin wax) (*26*, *29*–*31*) are some of the techniques that have been explored so far. Most combustion and chemical reaction techniques are irreversible; therefore, the fuel should be replenished after several cycles. In contrast, phase change materials can reversibly generate volumetric expansion.

In this work, we are proposing a simple method for generating the required pneumatic pressure inside a McKibben-type artificial muscle and soft robotic grippers without the use of compressors, pumps, and valves. The method involves generating high-pressure gas via inductively heating a ferromagnetic material in a liquid (e.g., water) with a small and portable high-power induction heater. Induction heating has already been used to heat thermo-sensitive polymers such as poly-*N*-isopropyl acrylamide doped with magnetic particles (*32*, *33*). We use this technique to generate pressure for pneumatic actuators.

In the water liquid-to-gas phase transition, the volume expands by a factor of 1600 at an atmospheric pressure, which is among the highest for liquids. By harnessing this significant volumetric expansion, we could demonstrate strains of up to 20% and work density of 40 kJ/m^3 with our magnetically induced thermal PAM (MITPAM); these results are similar to the peak energy density of skeletal muscle (*1*). Moreover, we demonstrated that, by using an engineered fluid with a boiling point of 61°C, we could actuate soft robotic grippers powered by only two Li-ion batteries.

RESULTS

Magnetothermal McKibben artificial muscle

Metallic particles such as ferrimagnetic nanoparticles (e.g., Fe_3O_4) (MNPs) generate heat when exposed to a high-frequency alternating magnetic field. The physics behind this phenomenon can be explained by different mechanisms, such as hysteresis losses, Joule heating via eddy current, Brownian relaxation, and Néel relaxation

[1]Koch Institute, Massachusetts Institute of Technology, Cambridge, MA 02139, USA. [2]Department of Electrical and Computer Engineering, Advanced Materials and Process Engineering Laboratory, University of British Columbia, Vancouver, BC V6T 1Z4, Canada. [3]BioInstrumentation Lab, Mechanical Engineering Department, Massachusetts Institute of Technology, Cambridge, MA 02139, USA. [4]Department of Chemical Engineering, Massachusetts Institute of Technology, Cambridge, MA 02139, USA. [5]Division of Health Science and Technology, Massachusetts Institute of Technology, Cambridge, MA 02139, USA. [6]Institute for Medical Engineering and Science, Massachusetts Institute of Technology, Cambridge, MA 02139, USA.
*Corresponding author. Email: seyed@mit.edu

Downloaded from https://www.science.org at The Hong Kong University of Science and Technology (Guangzhou) on May 26, 2026

(see the "Working mechanism" section in the Supplementary Materials). Our investigations revealed that hysteresis heating is the dominant heating mechanism for the MNPs/ferromagnetic rods that we used in this work (see the "Working mechanism" section in the Supplementary Materials).

To use the magnetothermal effect to actuate PAMs such as the McKibben artificial muscle, we filled a latex balloon with an MNPs/deionized water mixture (Materials and Methods). The balloon was then confined with a braided sleeve made of carbon fibers. Upon excitation with a high-frequency alternating magnetic field, the water mixture increases in temperature and generates steam, which develops positive pressure inside the system. Because of the confinement of the balloon with the braiding, the volumetric expansion of the balloon translates into an axial contractile strain and radial expansion (Fig. 1).

We used commercially available iron oxide–based MNPs (Materials and Methods). Scanning electron microscopy (SEM) analysis suggests a diameter range of 100 to 300 nm for the nanoparticles (Fig. 2A). An x-ray powder diffraction (XRD) analysis confirmed that the compound composition is magnetite (Fe_3O_4) (Fig. 2B). The MNPs are the essential ingredients in our design, because they are the energy converting units. Therefore, the more efficiently the MNPs convert the alternating magnetic field to heat, the lower the input electric power needed, which enhances the overall efficiency of the system. Magnetization plays an important role in determining the heat generation rate. The better the magnetization, the more heat can be generated. We measured a direct current (DC) magnetization of 47 electromagnetic units/g for the magnetite MNPs, which is very similar to the reported values in the literature (Fig. 2C) (*34*). By exciting 197 mg of the MNPs at an input power of 900 W, we could measure a temperature increase of 200°C with a heating rate of 20°C/s (Fig. 2D). This relatively high heating rate enabled us to achieve higher strain rates. We measured a strain rate of 1.2%/s, which is higher than that of any McKibben muscle filled with phase-changing–based materials (<<1%/s) (*26*, *31*). Combined with the high output stress, this strain rate enables the application of such actuators in robotic arms. Thanks to the high surface-to-volume ratio of the nanoparticles, a higher rate of steam formation could be achieved compared with the case of using a solid wire coiled inside the system. We found that heating the MNPs/water mixture occurs almost uniformly, which explains the increasing rate of steam formation. In the case of using a coiled wire, however, part of the heat transfers via convection or conduction in the phase-changing material. Using a solid wire as a heating element adds to the stiffness of the actuator, which, in turn, decreases the contractile strain. Moreover, encapsulating the system for high-pressure conditions is much easier without passing a heating wire through the structure.

As an illustrative example to demonstrate the generation of steam pressure inside the muscle, we filled a glass vial with MNPs/water mixture and sealed it with a latex balloon. When excited, the mixture generated enough pressure to inflate the balloon (Fig. 3A). We found that a pneumatic pressure of 2.1 ± 0.44 kPa is required to inflate the same type of balloon to a similar volume that was inflated with the magnetothermal excitation. To prevent the balloon from bursting, we excited the system at input powers less than 100 W. In this experiment, the heat transfer between the balloon and the environment prevents further inflation of the balloon but still clearly demonstrates the mechanism.

We achieved 20% contractile strain (in 10 s) under 2 kg of load, which is comparable to what can be achieved with a high-pressure air McKibben artificial muscle (Fig. 3, B and C) (*35*). The cooling time of the muscle in the relaxation state is on the order of tens of seconds (Fig. 3D). The cooling process can be a rate-limiting factor; however, we observed that it allows us to achieve a higher strain rate in successive excitations (Fig. 3E). As Fig. 3D suggests, the actuator's cooling profile in the "off" state consists of two regions. In the first region, occurring right after the power is switched off, the temperature drops rapidly to around the boiling point (i.e., a 50°C drop in less than 3 s), which results in a fast drop in strain. This drastic temperature drop allows the actuator to relax to its natural state faster, while its temperature is well above the room temperature. This thermal energy can be harnessed in the next excitation cycle to save some heating time. In other words, the actuation response time

Downloaded from https://www.science.org at The Hong Kong University of Science and Technology (Guangzhou) on May 26, 2026

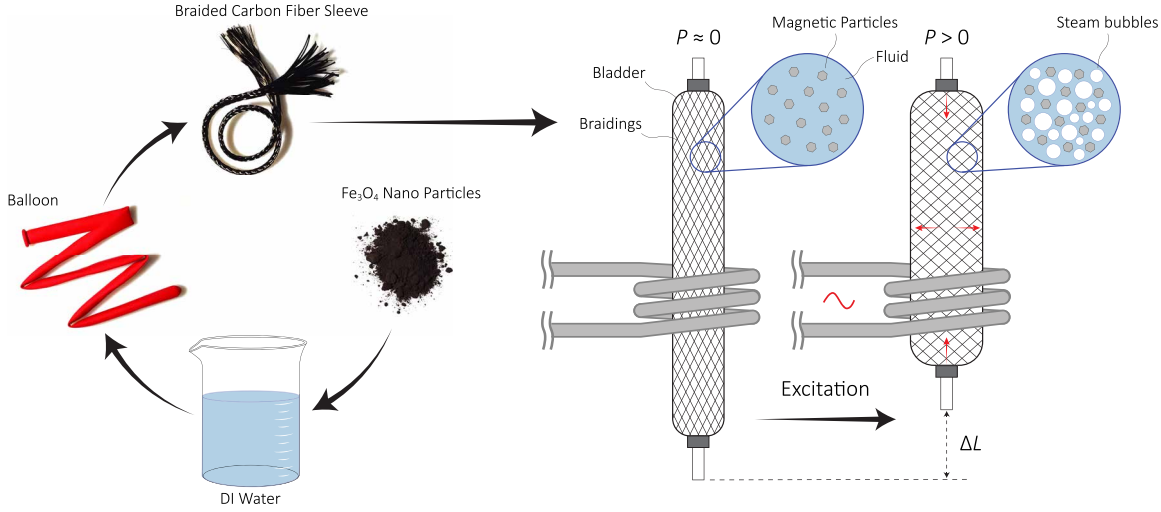

Fig. 1. Fabricating a MITPAM. MNPs are first mixed with deionized water, and the resulting mixture is then added to the balloon. The open end of the balloon is then sealed with a knot. The braided carbon fiber sleeve is then jacketed on the balloon. Upon excitation with a high-frequency (150 kHz) magnetic field, steam bubbles form and generate a significant pressure, *P*. The braiding translates the generated pressure to an axial contractile strain and radial expansion, resulting in a change in the length of the balloon, ΔL.

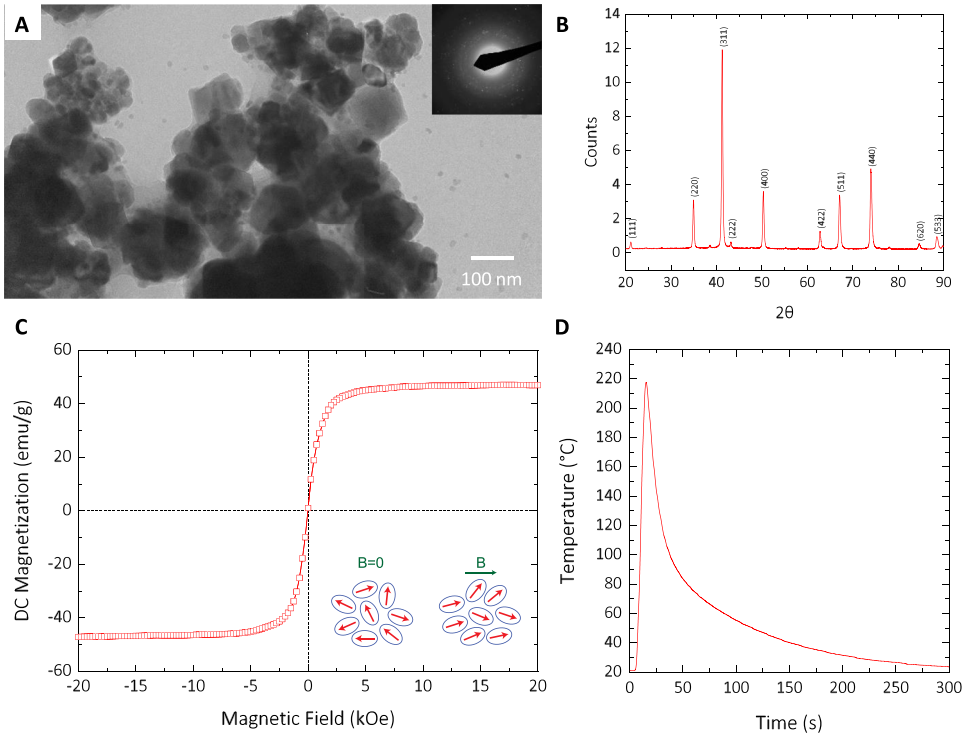

Fig. 2. Characterization of the MNPs. (**A**) SEM image of the MNPs showing particle size variation between 100 and 300 nm. (Inset) Selected area electron diffraction patterns. (**B**) XRD analysis indicates that the MNPs are magnetite (Fe_3O_4). (**C**) DC magnetization of the magnetite MNPs. (**D**) For the specific absorption test, 197 mg of the magnetite sample was excited at an input power of 900 W.

can be enhanced by maintaining the actuator's fluid temperature right below its boiling point in the relaxation state.

We further evaluated the performance of the muscle by measuring the blocking force (F_{block}) under isometric conditions (see the "Modeling" section in the Supplementary Materials). The blocking force profile was measured to be very similar to the temperature profile, which makes controlling the output force easier for robotic applications (Fig. 3F). To better understand the working mechanism of the muscle, we developed a model that uses temperature (T) and strain (ϵ) to predict the output force from the following equation (details of the derivation in the "Modeling" section in the Supplementary Materials)

$$F(T,\epsilon) = (\pi r_o^2)\left[\gamma(T-T_o) - \frac{1}{\kappa}\ln\left(b(1-\epsilon) - \frac{a}{3}(1-\epsilon)^3\right)\right][a(1-\epsilon)^2 - b] \quad (1)$$

where T_o is the temperature at which the pressure and volume are at their relaxed states (at the onset of actuation), r_o is the initial radius of the muscle, $a = 3/\tan^2(\theta_o)$ and $b = 1/\sin^2(\theta_o)$ are functions of the initial bias angle of the braiding (θ_o), and γ and κ are thermal pressure coefficient and coefficient of compressibility, respectively (see the "Modeling" section in the Supplementary Materials). This model is developed under the assumption of full transmission of the pressure inside the bladder to the external braiding without considering the stiffness of the muscle and geometry variations at both ends of the muscle.

Equation 1 describes the force-strain characteristics of the actuator. As illustrated in Fig. 4A, the output force is a function of the strain and the temperature. Therefore, under different stress or strain conditions, it can be in different states on the curves. For example, to move from the relaxed state O to A and then B, the temperature of the muscle should increase under an isometric condition (constant volume/strain). While transitioning from state B to C, under constant T, the load should decrease to obtain a higher strain. On the other hand, from state C to A, the strain decreases under an isotonic (constant load) condition and isometric condition for the state change of C to D when the excitation temperature (T) decreases.

Temperature (T) itself is a function of multiple parameters—such as the specific loss power (P), heat capacity (C), and heat loss coefficient (L)—as the following equation suggests (see the "Modeling" section in the Supplementary Materials)

$$T(t) = T_o + \Delta T_\infty 1(1 - \exp(-t/\tau)) \quad (2)$$

where $\Delta T_\infty = P/L$, $\tau = C/L$, and $T_\infty = T_o + \Delta T_\infty$. The specific loss power in hysteresis heating is proportional to the magnetization (M), magnitude (H), and frequency (f) of the applied magnetic field and the mass density (ρ_m) of the MNP/water mixture (see the "Modeling" section in the Supplementary Materials). The temperature (T) in Eq. 1 can be substituted with Eq. 2 to find the transient response of the system in an isotonic or isometric mode.

From the geometry of the braiding, an angle can be derived analytically at which the axial contractile strain becomes zero, and above that, the axial contractile strain turns into expanding strain. This angle, often called "magic angle," is $\theta_m = 54.74°$ and is typically used as the bias angle for the reinforcement braids used in garden hoses. One important implication of this magic angle in actuation performance is that—for the same excitation conditions and sample material—the farther the initial bias angle is away from this number, the more strain/stress it can generate. On the contrary, for a similar braiding type and length, the braiding with a smaller initial bias angle confines a smaller volume. Thus, lower steam pressure is generated during wireless excitation. In this work, we studied samples with braiding bias angles of 30° to 40°.

To determine the γ, first, we measured the blocking force (F_{block}) under isometric conditions (Fig. 4A) and converted it to pressure by setting $\epsilon = 0$ in Eq. 1 to obtain (see the "Modeling" section in the Supplementary Materials)

$$F_{block} = F(T,\epsilon)\,|_{\epsilon=0} = (\pi r_o^2)[\gamma(T-T_o)][a-b] \quad (3)$$

which gives $\Delta P = \gamma(T - T_o)$. We estimated the γ from the slope of the differential pressure (ΔP) versus temperature (T) curve to be around 5.1 kPa/K (Fig. 4B). Similarly, by increasing the temperature under isotonic conditions, we found the α from the slope of the normalized change in volume ($\Delta V/V_o$) versus temperature (T) (Fig. 4C)

Downloaded from https://www.science.org at The Hong Kong University of Science and Technology (Guangzhou) on May 26, 2026

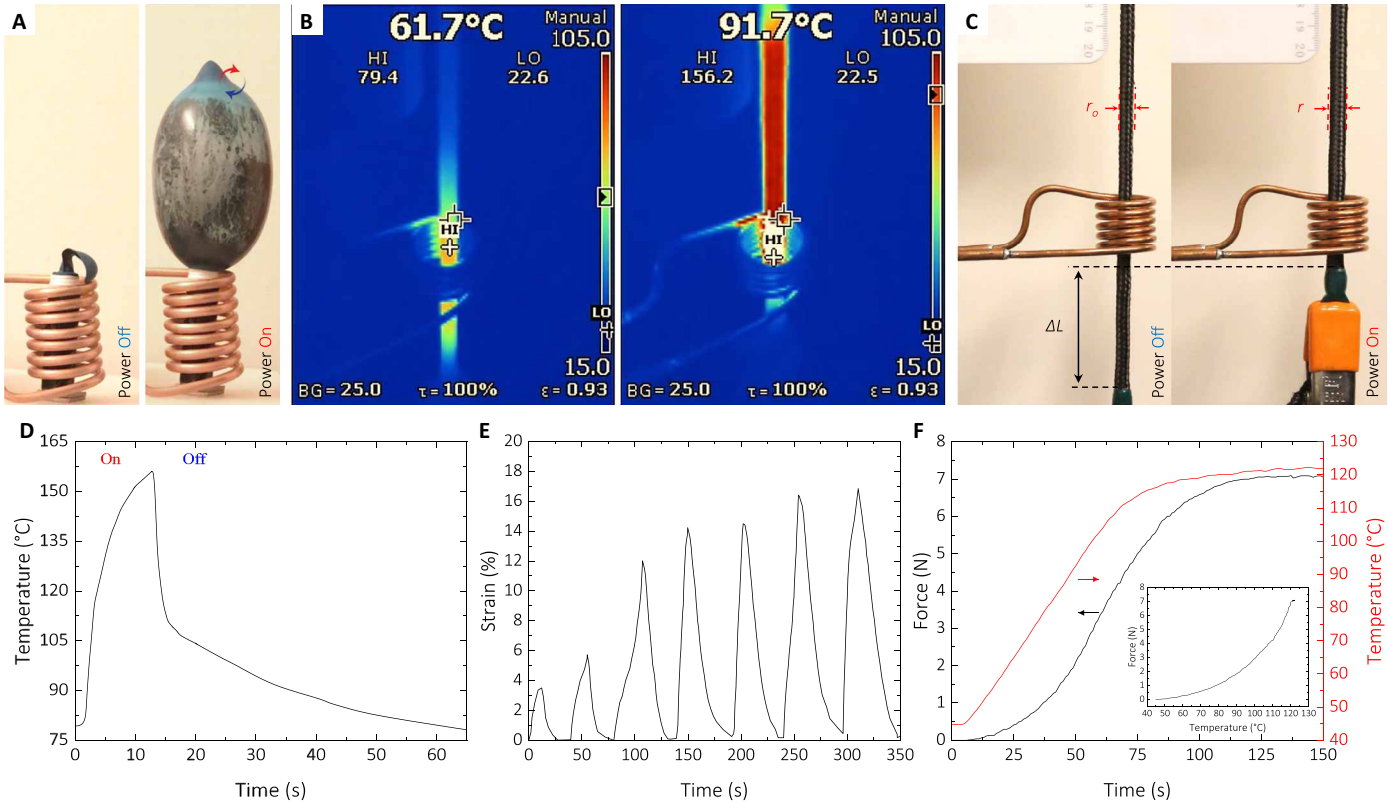

Fig. 3. Force, strain, and temperature response of a MITPAM. (**A**) Photograph illustrating the pressure generated inside the balloon during excitation. The outer diameter of the copper coil is 38 mm. (**B**) Thermal images of the actuator in (A) before (left) and after (right) excitation. (**C**) Before (left) and after (right) excitation of a MITPAM actuator under a 2-kg load generating 20% strain. (**D**) Temperature profile of the sample during on-off cycles. (**E**) Strain curve for multiple cycles. The first cycles are still warming up, whereas the last cycles have reached a steady-state peak strain. (**F**) Temperature and blocking force profiles as a function of time for a sample under isometric conditions. (Inset) The force response to the increase in temperature.

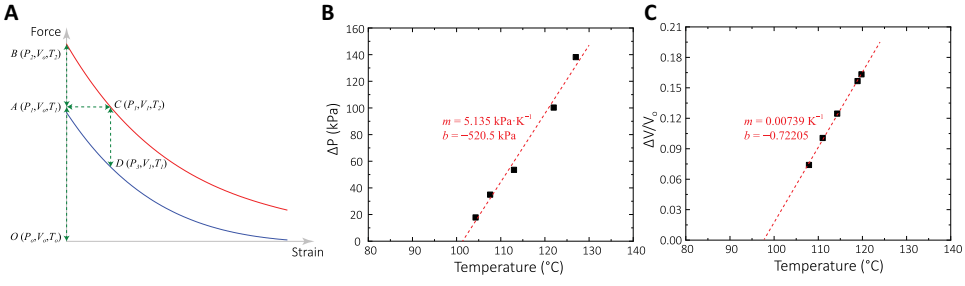

Fig. 4. Thermodynamics of the MITPAM. (**A**) Illustration of force versus strain for the MITPAM excited at temperatures T_1 and T_2. (**B**) Change in the pressure as a function of the maximum temperature. (**C**) Normalized volume change as a function of the maximum temperature.

(see the "Modeling" section in the Supplementary Materials). To evaluate the model, we made two samples with different initial bias angles and mixture concentrations. Sample 1, with an initial bias angle of 34.8° and a mixture concentration of 0.2 g/ml, generated less strain under no load, whereas sample 2, with a bias angle of 40° and a mixture concentration of 0.1 g/ml, generated larger strain under no load and smaller force at zero strain. The model was fitted to our experimental data by measuring the T, T_o, θ_o, γ, and κ experimentally (Fig. 5A) (see the "Modeling" section in the Supplementary Materials).

In robotics, it is sometimes desirable to lock the muscle after the first excitation without consuming further energy. In nature, spider dragline silk undergoes this dynamic at high-humidity conditions. The dragline silk super contracts (50% strain under no load) and maintains it (*1*). Some aquatic organisms, such as mollusks, have muscles that also exhibit such a property—called catch state or lockup state (*1*). To obtain such a property in the MITPAMs, instead of using water, we used carbonated water to make the mixture. Upon excitation, aside from generating steam, mixture effervesces and releases the dissolved carbon dioxide, which adds to the steam pressure. We achieved a strain locking of 2.5%, which is 22% of the value for the active strain (Fig. 5B). The actuator can relax back to its relaxed state by depressurizing the muscle by utilizing a valve. This feature can be used in situations where it is desired to lock or grip on an object for long periods without consuming further energy.

To evaluate the reproducibility of the strain, after the muscle reached a stable strain response, we excited the muscle for 50 more cycles. We did not observe any significant degradation in the strain (Fig. 5C). Considering the combination of strain and stress that the muscle can generate, we believe that it can be a good candidate for robotic applications. As a demonstration, we made a robotic arm and connected the MITPAM muscle in a configuration similar to

Downloaded from https://www.science.org at The Hong Kong University of Science and Technology (Guangzhou) on May 26, 2026

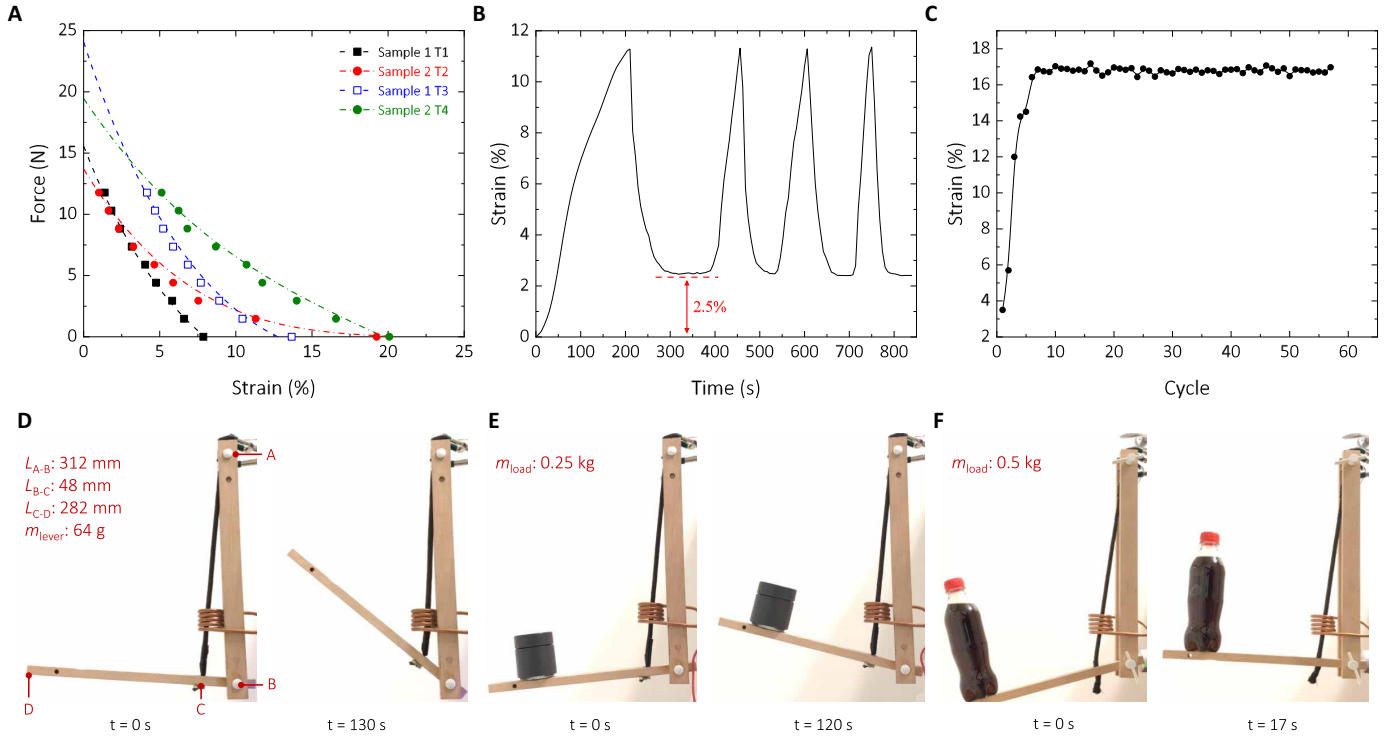

Fig. 5. Modeling and demonstration of robotic arm actuation. (**A**) Force-strain relationship through model and experimental data for two samples with different initial bias angles and mixture concentrations excited at two different temperatures. (**B**) Demonstration of locking strain or locking contraction after the first cycle with carbonated water. (**C**) Peak strain evolution through 50 successive excitations. (**D** to **F**) Before excitation (left) and after excitation (right) of the arm without any load (D), with a 250-g load (E), and with a 500-g load (F).

how the human biceps are connected to the elbow. We tested the performance of the muscle under no load, 250-g load, and 500-g load, which could generate torques of 0.1, 0.8, and 1.5 N·m, respectively (Fig. 5, D to F). The generated torque values translate to forces of 2.1, 16.5, and 31 N for Fig. 5 (D to F, respectively). The results suggest that the muscle can indeed be used for robotic applications.

The core working mechanism of our proposed actuation mechanism is based on the liquid-to-gas phase transition of a liquid via induction heating. The energy efficiency of the system was estimated to be <1%, which is within the range of efficiency for other thermal actuator technologies (see the "Energy analysis" section in the Supplementary Materials). However, the use of such an actuation mechanism can be justified when high output forces are desired from an untethered actuator.

Magnetothermal soft robotics

Our proposed idea of generating heat wirelessly can potentially be applied to different actuator technologies and even soft robots. To examine such integration, we used our actuation technique in the design of soft robotic grippers and fingers. Because of the geometry of the grippers, we decoupled the pressure-generation mechanism from the body of the actuator. To achieve this goal, instead of using MNPs and water, we used ferromagnetic rods (e.g., nails) and an engineered fluid with a boiling point of 61°C (see the "Energy analysis" section in the Supplementary Materials). Figure S1 illustrates the components and the schematic of the electronics that we used to make the magnetothermal soft grippers. The fabrication details of the soft grippers are provided in Materials and Methods.

We excited the soft grippers with two Li-ion batteries (fig. S1). We pulse width–modulated the input voltage to the induction heater with duty cycles of 100 (i.e., DC), 80, and 10% to control the pressure developed inside the actuator. As illustrated in Fig. 6A, the actuator was excited with an 80% duty cycle first, and when it reached the desired position, the duty cycle was reduced to 10% to hold it in place. The excitation pattern was repeated to demonstrate the controllability of the mechanism. In DC excitation, the actuator was excited until it grabbed an object and then was turned off (Fig. 6, B to D). One important aspect of this approach is that we could successfully demonstrate that the soft gripper can be actuated with two Li-ion batteries.

Heat management in thermal actuation plays a crucial role in determining the actuation rate. Thermal mass, heat conductivity of the materials, and cooling mechanism are the three major parameters that define actuation performance. Aside from engineering the materials' properties, the cooling rate can be reduced by scaling down the actuator size. To examine the scalability, we fabricated grippers of different sizes and actuated them with different volumes of the engineered fluid (i.e., 3, 15, and 50 ml) (Materials and Methods). The gripper filled with 3 ml of fluid exhibited an actuation response time of 10 s with a cooling time of 150 s, whereas the gripper filled with 50 ml of fluid showed an actuation response time of 130 s with a cooling time of more than 300 s. Therefore, we can confidently deduce that the actuation rate is inversely proportional to the size of the actuator. However, the output force generated by the actuator directly scales with its size.

We used high-frequency alternating current (AC) magnetic fields to boil a liquid and generate pressure inside a pneumatic actuator. It has been demonstrated that soft and thin materials can be coated

Downloaded from https://www.science.org at The Hong Kong University of Science and Technology (Guangzhou) on May 26, 2026

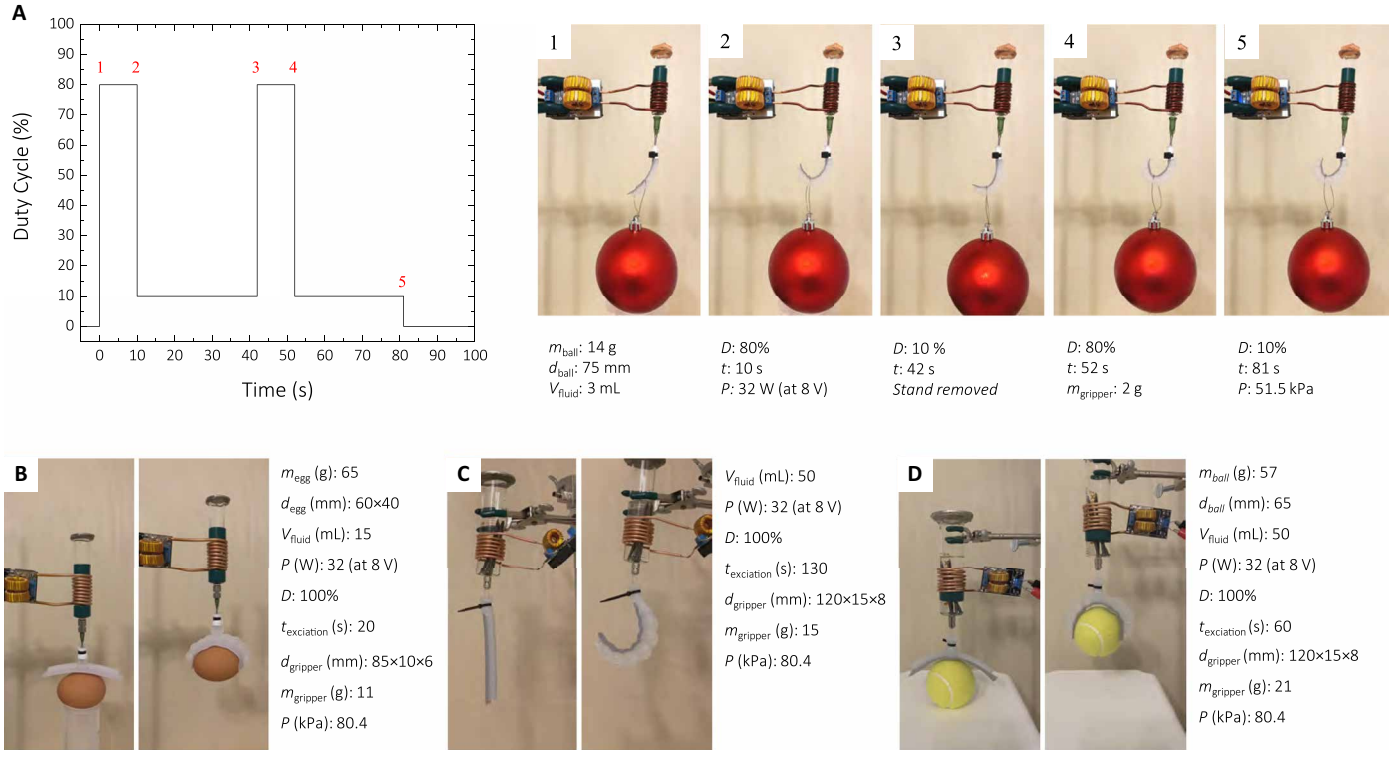

Fig. 6. Soft gripper demonstration. (**A**) Pulse width modulation control of a magnetothermally actuated soft gripper. The input power was pulse width–modulated to control the position of the gripper. In the first excitation cycle, the gripper was excited at 80% duty cycle, followed by a 10% duty cycle to prevent bursting. After 32 s of cooling, the gripper was excited with the same duty cycle pattern again. (**B** to **D**) DC excitation of a soft gripper: A cooked egg and a tennis ball were used as objects in experiments in (B) and (D). (C) The orange color object is a clamp that connects the actuator to the load. (D) The excitation time for this particular case was timed right before the bending of the gripper occurs. In all grippers, the mass of the connector is included in the mass of the gripper.

with permanent micromagnets and actuated with DC magnetic fields (*36*, *37*). One of the advantages of using a DC magnetic field is the fast response time that it can provide. This fast response time often translates to a high-power density actuation dynamic. However, the generated force by a magnetic field is a function of r^{-2}, which often leads to a small energy density actuation dynamic when the distance (e.g., r) is considerably large. In contrast, because of the nature of heating (e.g., heat capacity), excitation with AC magnetic field has the advantage of generating large forces but with slow actuation rates.

CONCLUSION

In the present work, we introduced an approach for operating McKibben-type artificial muscles and soft robotic grippers. This method involved generating the pneumatic pressure required for actuation via inductively boiling a liquid inside the actuator. With our design, we generated comparable performance results with the original tethered McKibben artificial muscle. MITPAM is compact and operates silently without relying on bulky and heavy air compressors, pressurized gas tanks, and valves. We demonstrated a 20% peak strain with a work density of 40 kJ/m^3, which is similar to what a skeletal muscle can generate.

In addition, we showed that our proposed mechanism is scalable and can be used in the design of soft robotic grippers. One of the benefits of the scalability is the reduction in power consumption, to the point that the actuator can be powered with only two lithium-ion batteries, which is very desirable for untethered applications, such as using the actuator in a confined and remote environment where no power transmission line is readily available.

One of the advantages of our proposed technique is that the generated heat by magnetic excitation can be easily controlled by adjusting the input power. Moreover, operating the fluid at around its boiling point enables significant pressure changes over a small temperature range. By controlling the Curie temperature (T_C) of the MNPs and ensuring that the hysteresis loss mechanism is the dominant heating mechanism, thermoregulation can be achieved to prevent excess heating of the MNPs. Miniaturization of the actuator, application of the mechanism to other actuator geometries, and engineering the phase transition liquid for lower operating temperatures are some of the remaining challenges for the future.

MATERIALS AND METHODS

Muscle characterization

The energy density is defined as the energy that is converted in a full contraction over the volume of the loaded muscle. The strain is defined as the change in length upon excitation normalized to the initial length of the loaded muscle.

Power and control components

The power and control components for exciting the soft robotic grippers consist of a microcontroller (e.g., Arduino Nano), a MOSFET power driver, a miniature induction heater, two Li-ion batteries (Samsung 30T 21700, 3000 mAh, 35 A), and a magnet wire coil

Downloaded from https://www.science.org at The Hong Kong University of Science and Technology (Guangzhou) on May 26, 2026

(fig. S1A). The total cost of the mentioned electronics with the glass syringe, ferromagnetic rod, and the fluid used for the soft gripper robotic experiments was about $59 (fig. S1A).

Magnetothermal artificial muscle preparation

We dispersed 1 to 2 g of magnetite powder (black iron oxide Fe_3O_4; Synthetic, Alpha Chemicals) in 7 to 10 ml of water by shaking the solution for 5 min. The optimal mass concentration of 200 mg/ml was obtained through back-of-envelope calculations and trial-and-error iterations to optimize for the volume of the bladder. Too low a concentration results in inefficient heating, and too high a concentration can cause thermal damage to the bladder and even generate small strains due to the lack of available fluid. For the strain-locking experiment, carbonated water (Schweppes carbonated water) was used instead of regular water. A latex balloon (260Q Twisting Balloons) was then filled with the dispersion and sealed with a knot. A braided carbon fiber sleeve with an inner diameter of 0.250 inches (6.35 mm) (ACP Composites Inc.) was used to confine the balloon. To facilitate the jacketing process, we lubricated the surface of the balloon with oil (Masters Lubricating Oiler). Both ends of the braiding were closed to confine the balloon along the length as well.

Temperature measurement

Sensors that have conductive wires, such as thermocouple or thermistors, are not immune to RFI (radio frequency interference), EMI (electromagnetic interference), nuclear magnetic resonance, and microwave radiation. To overcome this issue, we used a fiber-optic temperature sensor (Optocon FOTEMP1-OEM) and a thermal imaging camera (Fluke Ti100) instead.

Induction heating coil

We used a 1-m-long copper pipe with an outer diameter of $^3/_{16}$ inches (4.7625 mm) and a wall thickness of 0.03 inches (0.762 mm) to make the induction heating coil. The coil has 4.5 turns (N) with a coil length (L) of 30 mm and an inner diameter of 27.5 mm (R) (fig. S2A). For high-power excitations of the copper pipe coil, water circulation, at a constant temperature of 15°C, was used to cool down the coil during the excitation. For low excitation powers (<50 W), we used a magnet wire coil with a miniature induction heater (fig. S1).

Excitation apparatus

The induction heating apparatus is based on a zero voltage switching topology. Soft switching is used to reduce the voltage/current stress on the MOSFET during on/off transitions by using a MOSFET that has a fast-body diode across its drain and source (fig. S2B). The MNPs are represented as an LC circuit in the circuit diagram, with R and L representing a heating element and magnetic induction element, respectively. Two induction heaters with similar architectures were used, one for excitation powers of above 50 W (fig. S2) and one for below 50 W (fig. S1).

Coil characterization

A magnetic probe (model 100C; Beehive Electronics) and a spectrum analyzer (DSA815; RIGOL) were used to measure the magnetic field along the coil axis. Because of the attenuation limits on the spectrum analyzer and induction heating of the magnetic field probe at high magnetic fields, it was not possible to measure the magnitude of the magnetic field inside the coil. Therefore, we measured the magnetic field from 150 to 20 mm with reference to the edge of the coil and used the governing physical models to find the H in the center of the coil. We formulated the magnetic field as a function of distance from the center of a coil of width dw from the Biot-Savart as mentioned below

$$\mathrm{d}B_x = \frac{\mu_o(nI\mathrm{d}w)}{2}\frac{R^2}{\left[(x-w)^2+R^2\right]^{3/2}} \tag{4}$$

where $n = N/L$ is the number of turns per length of the coil, R is the radius of the ring, and I is the current through the ring (fig. S3A). Integrating Eq. 4 from $a = -L/2$ to $b = L/2$, we find the B_x to be

$$B_x = \frac{\mu_o nI}{2}R^2\int_a^b \frac{1}{\left[(x-w)^2+R^2\right]^{3/2}}\mathrm{d}w = \frac{\mu_o nI}{2}\left(\frac{x-a}{\sqrt{(x-a)^2+R^2}} - \frac{x-b}{\sqrt{(x-b)^2+R^2}}\right) \tag{5}$$

We can determine the magnetic field in the center of the coil to be

$$B_{x=0} = \mu_o nI\frac{L}{\sqrt{L^2+4R^2}} \tag{6}$$

The current (I) in Eq. 5 was found by measuring the voltage across the coil and using the following equation (assuming zero resistance across the coil) for impedance to find the current

$$I = \frac{V}{2\pi fL} \tag{7}$$

where L is the inductance of the coil, which can be found from the resonance frequency of the LC tank [i.e., $L = 1/C(2\pi f)^2$]. By using the measured data for the amplitude of the magnetic field as a function of distance, we can fit Eq. 5 to estimate the magnetic field inside the coil to be $H \approx 3$ kA/m and $H \approx 9$ kA/m for excitation voltages of 12 and 33 V, respectively (fig. S3B). By using the parameters found from fitting Eq. 5 to the experimental data, we can find the magnetic field strength in the center of the coil as a function of the input power (fig. S3C).

Soft robotic gripper

The soft grippers were fabricated through a molding process. The mold (fig. S4A) was three-dimensionally (3D) printed with a fused deposition modeling 3D printer (FlashForge Creator Pro) with a 0.1-mm-layer resolution and a print resolution of 0.2 mm. Polylactic acid thermoset filament (1.75 mm in diameter) was used to print the objects in a temperature-controlled chamber. Three different molds were fabricated to examine the scalability of the magnetothermal actuator (fig. S4B).

EcoFlex 00-50 platinum-catalyzed silicone rubber was used as the body material for the soft grippers. The low elastic modulus (83 kPa) and significant elongation at break (980%) make the EcoFlex an excellent material for the application in soft robotics. The material was prepared by mixing a one-to-one ratio of the two precursors, followed by degassing the mixture in a desiccator for 5 min. A rotary vacuum pump was used to generate the required vacuum in the desiccator. The mixture was then transferred to the molds and degassed further in the desiccator and cured at 65°C for 10 min. To prevent the gripper side of the actuator from expanding, a piece of

Downloaded from https://www.science.org at The Hong Kong University of Science and Technology (Guangzhou) on May 26, 2026

cotton fabric was adhered to it by coating the fabric with EcoFlex 00-50. The cotton fabric was chosen because of its porous property, which allowed it to act as a good adhesion layer to the gripper. Moreover, fabrics are flexible and exhibit the required planar stiffness for this purpose. The inlet channel to the gripper was molded separately and attached to the gripper by using another application of EcoFlex 00-50.

SUPPLEMENTARY MATERIALS

robotics.sciencemag.org/cgi/content/full/5/41/eaaz4239/DC1
Working mechanism
Modeling
Energy analysis
Fig. S1. The hardware schematic for magnetically induced thermal soft robotic grippers.
Fig. S2. The circuit diagram for MITPAM.
Fig. S3. Measured data and simulation results for magnetic field strength inside the coil.
Fig. S4. The specs for the molds used to fabricate the soft robotic grippers.
Fig. S5. Illustration of the response of various types of magnetic particles under magnetic field.
Fig. S6. Characterization of the MNPs based on their thermal response to various magnetic field strengths.
Table S1. Heat parameters of the fluids used in this work.
Movie S1. Magnetothermal actuation of a MITPAM demonstrating 20% strain under a 2-kg load excited at an input power of 900 W.
Movie S2. MITPAM robotic arms under no load.
Movie S3. MITPAM robotic arms under a 250-g load.
Movie S4. MITPAM robotic arms under a 500-g load.
Movie S5. Lifting an egg by magnetothermal actuation of a soft gripper.
Movie S6. Lifting a ball by magnetothermal actuation of a soft gripper.
Movie S7. Controlled magnetothermal actuation of a soft gripper.
References (*38*–*41*)

REFERENCES AND NOTES

1. S. M. Mirvakili, I. W. Hunter, Artificial muscles: Mechanisms, applications, and challenges. *Adv. Mater.* **30**, 1704407 (2018).
2. S. M. Mirvakili, I. W. Hunter, Fast Torsional artificial muscles from NiTi twisted yarns. *ACS Appl. Mater. Interfaces* **9**, 16321–16326 (2017).
3. S. M. Mirvakili, I. W. Hunter, A torsional artificial muscle from twisted nitinol microwire. *Proc. SPIE* **10163**, 101630S1–101630S7 (2017).
4. A. Lendlein, H. Jiang, O. Junger, R. Langer, Light-induced shape-memory polymers. *Nature* **434**, 879–882 (2005).
5. R. Mohr, K. Kratz, T. Weigel, M. Lucka-Gabor, M. Moneke, A. Lendlein, Initiation of shapememory effect by inductive heating of magnetic nanoparticles in thermoplastic polymers. *Proc. Natl. Acad. Sci. U.S.A.* **103**, 3540–3545 (2006).
6. P. R. Buckley, G. H. Mckinley, T. S. Wilson, W. Small, W. J. Benett, J. P. Bearinger, M. W. Mcelfresh, D. J. Maitland, Inductively heated shape memory polymer for the magnetic actuation of medical devices. *IEEE Trans. Biomed. Eng.* **53**, 2075–2083 (2006).
7. E. Acome, S. K. Mitchell, T. G. Morrissey, M. B. Emmett, C. Benjamin, M. King, M. Radakovitz, C. Keplinger, Hydraulically amplified self-healing electrostatic actuators with muscle-like performance. *Science* **359**, 61–65 (2018).
8. C. Christianson, N. N. Goldberg, D. D. Deheyn, S. Cai, M. T. Tolley, Translucent soft robots driven by frameless fluid electrode dielectric elastomer actuators. *Sci. Robot.* **3**, eaat1893 (2018).
9. N. Kellaris, V. G. Venkata, G. M. Smith, S. K. Mitchell, C. Keplinger, Peano-HASEL actuators: Muscle-mimetic, electrohydraulic transducers that linearly contract on activation. *Sci. Robot.* **3**, eaar3276 (2018).
10. S. Sridar, C. J. Majeika, P. Schaffer, M. Bowers, S. Ueda, A. J. Barth, J. L. Sorrells, J. T. Wu, T. R. Hunt, M. Popovic, Hydro muscle—A novel soft fluidic actuator, in *IEEE International Conference on Robotics and Automation (ICRA)* (IEEE, 2016), pp. 4014–4021.
11. C. S. Haines, M. D. Lima, N. Li, G. M. Spinks, J. Foroughi, J. D. W. Madden, S. H. Kim, S. Fang, M. J. de Andrade, F. Goktepe, O. Goktepe, S. M. Mirvakili, S. Naficy, X. Lepro, J. Oh, M. E. Kozlov, S. J. Kim, X. Xu, B. J. Swedlove, G. G. Wallace, R. H. Baughman, Artificial muscles from fishing line and sewing thread. *Science* **343**, 868–872 (2014).
12. S. M. Mirvakili, I. W. Hunter, Multidirectional artificial muscles from nylon. *Adv. Mater.* **29**, 1604734 (2017).
13. R. H. Baughman, Conducting polymer artificial muscles. *Synth. Met.* **78**, 339–353 (1996).
14. K. Uh, B. Yoon, C. W. Lee, J.-M. Kim, An electrolyte-free conducting polymer actuator that displays electrothermal bending and flapping wing motions under a magnetic field. *ACS Appl. Mater. Interfaces* **8**, 1289–1296 (2016).
15. Y. Yan, T. Santaniello, L. G. Bettini, C. Minnai, A. Bellacicca, R. Porotti, I. Denti, G. Faraone, M. Merlini, C. Lenardi, P. Milani, Electroactive ionic soft actuators with monolithically integrated gold nanocomposite electrodes. *Adv. Mater.* **29**, 1606109 (2017).
16. Q. Shen, S. Trabia, T. Stalbaum, V. Palmre, K. Kim, I.-K. Oh, A multiple-shape memory polymer-metal composite actuator capable of programmable control, creating complex 3D motion of bending, twisting, and oscillation. *Sci. Rep.* **6**, 24462 (2016).
17. M. A. Robertson, H. Sadeghi, J. M. Florez, J. Paik, Soft pneumatic actuator fascicles for high force and reliability. *Soft Robot.* **4**, 23–32 (2016).
18. D. Yang, M. S. Verma, J.-H. So, B. Mosadegh, C. Keplinger, B. Lee, F. Khashai, E. Lossner, Z. Suo, G. M. Whitesides, Buckling pneumatic linear actuators inspired by muscle. *Adv. Mater. Technol.* **1**, 1600055 (2016).
19. M. De Volder, A. J. M. Moers, D. Reynaerts, Fabrication and control of miniature McKibben actuators. *Sens. Actuators Phys.* **166**, 111–116 (2011).
20. E. W. Hawkes, D. L. Christensen and A. M. Okamura, Design and implementation of a 300% strain soft artificial muscle, in *IEEE International Conference on Robotics and Automation (ICRA)* Stockholm (IEEE, 2016), pp. 4022–4029.
21. L. Belding, B. Baytekin, H. T. Baytekin, P. Rothermund, M. S. Verma, A. Nemiroski, D. Sameoto, B. A. Grzybowski, G. M. Whitesides, Slit tubes for semisoft pneumatic actuators. *Adv. Mater.* **30**, 1704446 (2018).
22. S. I. Rich, R. J. Wood, C. Majidi, Untethered soft robotics. *Nat. Electron.* **1**, 102–112 (2018).
23. S. Li, D. M. Vogt, D. Rus, R. J. Wood, Fluid-driven origami-inspired artificial muscles. *Proc. Natl. Acad. Sci. U.S.A.* **114**, 13132–13137 (2017).
24. N. W. Bartlett, M. T. Tolley, J. T. B. Overvelde, J. C. Weaver, B. Mosadegh, K. Bertoldi, G. M. Whitesides, R. J. Wood, A 3D-printed, functionally graded soft robot powered by combustion. *Science* **349**, 161–165 (2015).
25. M. Wehner, R. L. Truby, D. J. Fitzgerald, B. Mosadegh, G. M. Whitesides, J. A. Lewis, R. J. Wood, An integrated design and fabrication strategy for entirely soft, autonomous robots. *Nature* **536**, 451–455 (2016).
26. A. Miriyev, K. Stack, H. Lipson, Soft material for soft actuators. *Nat. Commun.* **8**, 596 (2017).
27. T. M. Sutter, M. B. Dickerson, T. S. Creasy, R. S. Justice, Rubber muscle actuation with pressurized CO_2 from enzyme-catalyzed urea hydrolysis. *Smart Mater. Struct.* **22**, 094022 (2013).
28. B. Tondu, R. Emirkhanian, S. Mathé, A. Ricard, A pH-activated artificial muscle using the McKibben-type braided structure. *Sens. Actuators Phys.* **150**, 124–130 (2009).
29. Z. Zhou, Q. Li, L. Chen, C. Liu, S. Fan, A large-deformation phase transition electrothermal actuator based on carbon nanotube–elastomer composites. *J. Mater. Chem. B* **4**, 1228–1234 (2016).
30. B. Liu, Y. Hou, D. Li, J. Yang, A thermal bubble micro-actuator with induction heating. *Sens. Actuators Phys.* **222**, 8–14 (2015).
31. D. Sangian, S. Naficy, G. M. Spinks, Thermally activated paraffin-filled McKibben muscles. *J. Intell. Mater. Syst. Struct.* **27**, 2508–2516 (2016).
32. T. Shen, M. G. Font, S. Jung, M. L. Gabriel, M. P. Stoykovich, F. J. Vernerey, Remotely triggered locomotion of hydrogel mag-bots in confined spaces. *Sci. Rep.* **7**, 16178 (2017).
33. A. H. Mitwalli, T. A. Denison, D. K. Jackson, S. B. Leeb, T. Tanaka, Closed-loop feedback control of magnetically-activated gels. *J. Intel. Mat. Syst. Str.* **8**, 596–604 (1997).
34. V. A. J. Silva, P. L. Andrade, M. P. C. Silva, A. D. Bustamante, L. De Los Santos Valladares, J. A. Aguiar, Synthesis and characterization of Fe_3O_4 nanoparticles coated with fucan polysaccharides. *J. Magn. Magn. Mater.* **343**, 138–143 (2013).
35. Buy Fluidic Muscle DMSP online Festo USA (available at https://www.festo.com/rep/en_corp/assets/pdf/info_501_en.pdf).
36. M. M. Schmauch, S. R. Mishra, B. A. Evans, O. D. Velev, J. B. Tracy, Chained iron microparticles for directionally controlled actuation of soft robots. *ACS Appl. Mater. Interfaces* **9**, 11895–11901 (2017).
37. Y. Kim, H. Yuk, R. Zhao, S. A. Chester, X. Zhao, Printing ferromagnetic domains for untethered fast-transforming soft materials. *Nature* **558**, 274–279 (2018).
38. E. Natividad, I. Andreu, Characterization of magnetic hyperthermia, in *Magnetic Characterization Techniques for Nanomaterials*, C. S. S. R. Kumar, Ed. (Springer Berlin Heidelberg, 2017), pp. 261–303.
39. R. Hiergeist, W. Andra, N. Buske, R. Hergt, I. Hilger, U. Richter, W. Kaiser, Application of magnetite ferrofluids for hyperthermia. *J. Magn. Magn. Mater.* **201**, 420–422 (1999).
40. B. Tondu, P. Lopez, Modeling and control of McKibben artificial muscle robot actuators. *IEEE Control Syst. Mag.* **20**, 15–38 (2000).
41. K. Dill, S. Bromberg, *Molecular Driving Forces: Statistical Thermodynamics in Biology, Chemistry, Physics, and Nanoscience* (Garland Science, ed. 2, 2010).

Acknowledgments: We thank Y. Zhang, P. Boisvert, and C. Settens for assisting with the TEM imaging, magnetic characterization of the MNPs, and XRD measurements, respectively.
Funding: The authors acknowledge funding from Gates Foundation grant OPP1136638.
Author contributions: S.M.M. conceived and initiated the project, and designed and performed all experiments. D.S. conducted and contributed to the 3D printing design and experiments. S.M.M. and D.S. wrote the manuscript. I.W.H. and R.L. provided supervision. All

Downloaded from https://www.science.org at The Hong Kong University of Science and Technology (Guangzhou) on May 26, 2026

the authors read and commented on the manuscript. **Competing interests:** S.M.M., I.W.H., and R.L. are inventors on patent application 62/989,084 held/submitted by the Massachusetts Institute of Technology that covers the subject matter disclosed in this paper. D.S. does not have any competing interests. To the best of his knowledge, R.L. has no other competing interests in relation to this paper. For a complete list of R.L.'s general competing interest disclosures, please visit www.dropbox.com/s/yc3xqb5s8s94v7x/Rev%20Langer%20COI.pdf?dl=0. **Data and materials availability:** All data needed to evaluate the conclusions in the paper are present in the paper or the Supplementary Materials.

Submitted 8 September 2019
Accepted 16 March 2020
Published 15 April 2020
10.1126/scirobotics.aaz4239

Citation: S. M. Mirvakili, D. Sim, I. W. Hunter, R. Langer, Actuation of untethered pneumatic artificial muscles and soft robots using magnetically induced liquid-to-gas phase transitions. *Sci. Robot.* **5**, eaaz4239 (2020).

Downloaded from https://www.science.org at The Hong Kong University of Science and Technology (Guangzhou) on May 26, 2026

Science Robotics

Actuation of untethered pneumatic artificial muscles and soft robots using magnetically induced liquid-to-gas phase transitions

Seyed M. Mirvakili, Douglas Sim, Ian W. Hunter, and Robert Langer

Sci. Robot. **5** (41), eaaz4239. DOI: 10.1126/scirobotics.aaz4239

View the article online
https://www.science.org/doi/10.1126/scirobotics.aaz4239
Permissions
https://www.science.org/help/reprints-and-permissions

Downloaded from https://www.science.org at The Hong Kong University of Science and Technology (Guangzhou) on May 26, 2026

Use of this article is subject to the Terms of service

Science Robotics (ISSN 2470-9476) is published by the American Association for the Advancement of Science. 1200 New York Avenue NW, Washington, DC 20005. The title *Science Robotics* is a registered trademark of AAAS.

Copyright © 2020 The Authors, some rights reserved; exclusive licensee American Association for the Advancement of Science. No claim to original U.S. Government Works